NASA Contractor Report 181682

ICASE REPORT NO. 88-32

ICASE

A NAVIER-STOKES SOLVER FOR CASCADE FLOWS

A. Arnone

R. C. Swanson

Contract No. NAS1-18107
July 1988

INSTITUTE FOR COMPUTER APPLICATIONS IN SCIENCE AND ENGINEERING
NASA Langley Research Center, Hampton, Virginia 23665

Operated by the Universities Space Research Association

National Aeronautics and
Space Administration

Langley Research Center
Hampton, Virginia 23665

A NAVIER-STOKES SOLVER FOR CASCADE FLOWS

A. Arnone*
Institute for Computer Applications in Science and Engineering

R. C. Swanson
NASA Langley Research Center

ABSTRACT

A computer code for solving the Reynolds averaged full Navier-Stokes equations has been developed and applied using sheared H-type grids. The Baldwin-Lomax eddy-viscosity model is used for turbulence closure. The integration in time is based on an explicit four-stage Runge-Kutta scheme. Local time stepping, variable coefficient implicit residual smoothing, and a full multigrid method have been implemented to accelerate steady state calculations. Comparisons with experimental data show that the code is an accurate viscous solver and can give very good blade-to-blade predictions for engineering applications in less than 100 multigrid cycles on the finest mesh.

*This research was supported by the National Aeronautics and Space Administration under Contract No. NAS1-18107 while the first author was in residence at the Institute for Computer Applications in Science and Engineering (ICASE), NASA Langley Research Center, Hampton, VA 23665.

INTRODUCTION

The capability to correctly predict the various flow conditions that can occur in turbomachinery blade passages is a basic step for the design and the improvement of the modern compressors and turbines. As indicated by the research of the past few years, flow solutions can be obtained rapidly by solving the potential equation, but this equation does not allow for vorticity and entropy changes related to shock waves. Recently, many numerical methods have been developed which solve the Euler equations. However, an inviscid analysis requires some assumption about the circulation to get an unique solution, and the problem may become ambiguous when dealing with a rounded trailing edge. In addition, heat transfer and boundary-layer thickening, that can lead to separation and hot spots, cannot be represented in an inviscid solution.

By coupling a boundary-layer model with an inviscid procedure one can remove some of the previous limitations, but such an approach is difficult to extend to three-dimensional flows. The improvement in the numerical schemes and in the performance of modern computers suggests investigating the solution of the Reynolds averaged Navier-Stokes equations. Although significant progress has been made in the development of Navier-Stokes solvers for cascade flows, as evident from [1-3], much work remains before computer codes capable of efficiently solving the wide range of blade geometries and flow conditions that can be encountered in the design process are available.

The objective of the present work is to develop a fast and accurate method for the computation of viscous cascade flows. A four stage Runge-Kutta scheme with acceleration techniques for steady-state solutions is used to advance in time the Reynolds averaged Navier-Stokes equations. Numerical efficiency has been achieved through local time stepping, variable coefficient implicit residual smoothing, and a full multigrid method. Sheared H-type grids are used to discretize the computational domain. These grids are easy to generate algebraically and to extend to three-dimensional problems, and they generally provide sufficient resolution for engineering purposes.

In this paper, numerical results are presented for a bicircular arc cascade, for a typical gas turbine high loaded cascade with thick, rounded trailing edge, and for a bump in a channel. The bicircular profile is studied for the case of subsonic, laminar, separated flow and for the case of transonic, turbulent flow with separation at the foot of the shock and near the trailing edge. For the gas turbine blade, subsonic and transonic conditions are considered, and solutions are compared to experimental data. Finally, the capability of the present prediction technique to compute supersonic flows is demonstrated with the bump in a channel problem. For all these cases, convergence histories are shown.

GOVERNING EQUATIONS

Let ρ, u, v, p, T, E, and H denote respectively the density, velocity components in the x and y cartesian directions, pressure, temperature, specific total internal energy, and specific total enthalpy. The two-dimensional, unsteady Navier-Stokes equations, neglecting body forces and heat sources, can be written in conservative form in a cartesian coordinate system as,

$$\frac{\partial U}{\partial t} + \frac{\partial F}{\partial x} + \frac{\partial G}{\partial y} = \frac{\partial R}{\partial x} + \frac{\partial S}{\partial y} \tag{1}$$

where

$$U = \begin{bmatrix} \rho \\ \rho u \\ \rho v \\ \rho E \end{bmatrix}; \quad F = \begin{bmatrix} \rho u \\ \rho u^2 + p \\ \rho uv \\ \rho uH \end{bmatrix}; \quad G = \begin{bmatrix} \rho v \\ \rho uv \\ \rho v^2 + p \\ \rho vH \end{bmatrix} \tag{2}$$

$$R = \begin{bmatrix} 0 \\ \tau_{xx} \\ \tau_{xy} \\ r_4 \end{bmatrix}; \quad S = \begin{bmatrix} 0 \\ \tau_{yx} \\ \tau_{yy} \\ s_4 \end{bmatrix} \tag{3}$$

and

$$\begin{aligned} \tau_{xx} &= (\lambda + 2\mu)u_x + \lambda v_y \\ \tau_{yy} &= (\lambda + 2\mu)v_y + \lambda u_x \\ \tau_{xy} &= \tau_{yx} = \mu(u_y + v_x) \\ r_4 &= u\tau_{xx} + v\tau_{xy} + kT_x \\ s_4 &= u\tau_{yx} + v\tau_{yy} + kT_y. \end{aligned} \tag{4}$$

The pressure is obtained from the equation of state,

$$p = \rho RT. \tag{5}$$

According to the Stokes hypothesis λ is taken to be $-2/3\mu$ and a power law is used to determine the molecular coefficient of viscosity μ. The effect of turbulence is taken into account by using the eddy-viscosity hypothesis. That is, the molecular viscosity μ and the molecular thermal conductivity k are replaced with,

$$\mu = \mu_\ell + \mu_t \tag{6}$$

$$k = c_p \left[\left(\frac{\mu}{Pr} \right)_\ell + \left(\frac{\mu}{Pr} \right)_t \right] \tag{7}$$

where c_p is the specific heat at constant pressure, Pr is the Prandtl number, and the subscripts ℓ and t refer to laminar and turbulent. The turbulence quantities μ_t and Pr_t are computed using the two-layer algebraic model of Baldwin and Lomax [4].

The Euler equations can be easily obtained by neglecting the right hand side of equation (1).

SPATIAL DISCRETIZATION

A finite-volume approach is applied to discretize the equations of motion. The computational domain is divided into quadrilateral cells, fixed in time, and for each cell the governing equations are written in integral form as follows,

$$\frac{\partial}{\partial t}\int\int_{\Omega} U dxdy + \int_{\partial\Omega}(Fdy - Gdx) = \int_{\partial\Omega}(Rdy - Sdx) \tag{8}$$

where Ω is a generic cell and $\partial\Omega$ its boundary.

A cell-centered discretization is used, and the line integral of (8) is approximated with the midpoint rule. The convective fluxes at the cell faces are obtained by simple averaging of adjacent cell-center values of the dependent variables (see [5]). The spatial derivatives necessary to compute the viscous terms are evaluated by means of Green's theorem. For example, consider the arbitrary cell Ω (EFGH) in Fig. 1. The contributions u_x and u_y to the viscous flux across each cell face (i.e., GH) are determined using

$$\begin{aligned} \int_{\Omega'} u_x d\Omega' &= \int_{\partial\Omega'} u dy \\ \int_{\Omega'} u_y d\Omega' &= -\int_{\partial\Omega'} u dx \end{aligned} \tag{9}$$

where Ω' is an auxiliary cell (CGNH for face GH in Fig. 1). In a similar manner, v_x and v_y are computed. Additional details for finite-volume treatment of viscous stresses and heat conduction terms are found in [5] and [6].

BOUNDARY CONDITIONS

It is well-known that the reflective behavior of numerical boundary conditions can significantly influence the convergence rate of a marching scheme. Thus, boundary conditions must be chosen carefully. According to the theory of characteristics, three quantities are specified at a subsonic inflow boundary. In the present work, the total enthalpy, the total pressure, and flow angle are specified if the axial flow is subsonic; the outcoming Riemann invariant R^- is taken from the interior. For supersonic axial inlet all the flow variables are computed from the prescribed inlet conditions. At a subsonic axial outlet, the static

pressure corresponding to the desired isentropic Mach number is prescribed, while the outgoing Riemann invariant R^+, the total enthalpy, and the component of the velocity parallel to the boundary are extrapolated from the interior. If the axial outlet is supersonic all the variables are extrapolated. On the solid wall, the only contribution to the convective fluxes is the pressure, which is obtained by extrapolation from the interior of the flow field. For viscous flow calculations, the velocity is set to zero on the solid surface, which is taken to be adiabatic in the present work.

ARTIFICIAL DISSIPATION

For inviscid flows the finite-volume scheme does not contain any dissipative terms. In order to prevent odd-even point decoupling and oscillations near shock waves or stagnation points, artificial dissipation terms are added to the governing discrete equations. For viscous flows dissipative properties are present due to diffusive terms; however, away from shear layer regions (i.e., boundary layers, wakes) the physical dissipation may not be sufficient to guarantee stability, especially in the case of stretched meshes. Although shock waves can be captured by defining the shock structure and solving the full Navier-Stokes equations, the required mesh resolution is not practical. Thus, to maintain the stability and robustness of the numerical procedure, artificial dissipation is also included in viscous calculations. A semidiscrete form of (8) is then given by

$$\frac{\partial}{\partial t}(V \cdot U) + Q(U) - D(U) = 0 \tag{10}$$

where V is the volume of the mesh cell being considered, Q is the discrete operator for the convective and physical diffusive terms, and D is the operator for the artificial dissipative terms.

The artificial dissipation model considered in this paper is basically the one developed by Jameson, Schmidt, and Turkel [7]. This nonlinear model is a blending of second and fourth differences. The quantity $D(U)$ in (10) is defined as

$$D(U) = (D_\xi^2 - D_\xi^4 + D_\eta^2 - D_\eta^4)U \tag{11}$$

where (ξ, η) are arbitrary curvilinear coordinates,

$$D_\xi^2 U = \nabla_\xi(\lambda_{i+\frac{1}{2},j} \cdot \varepsilon^{(2)}_{i+\frac{1}{2},j})\Delta_\xi U_{i,j}, \tag{12}$$

$$D_\xi^4 U = \nabla_\xi(\lambda_{i+\frac{1}{2},j} \cdot \varepsilon^{(4)}_{i+\frac{1}{2},j})\Delta_\xi \nabla_\xi \Delta_\xi U_{i,j}, \tag{13}$$

i, j are indices (for a cell center) associated with the ξ and η directions, and Δ_ξ, ∇_ξ are forward and backward difference operators in the ξ direction. Following [6] and [8] the

variable scaling factor is defined as

$$\lambda_{i+\frac{1}{2},j} = \frac{1}{2}[(\overline{\lambda}_\xi)_{i,j} + (\overline{\lambda}_\xi)_{i+1,j}] \tag{14}$$

where

$$\begin{aligned} (\overline{\lambda}_\xi)_{i,j} &= \phi_{i,j}(r) \cdot (\lambda_\xi)_{i,j}, \\ \phi_{i,j}(r) &= 1 + r_{i,j}^{\varsigma}, \end{aligned} \tag{15}$$

r is the ratio λ_η/λ_ξ, λ_ξ and λ_η are the scaled spectral radii of the flux Jacobian matrices (associated with the ξ and η directions) for the Euler equations, and the exponent ς is generally defined by $\frac{2}{3} \leq \varsigma \leq 1$. The spectral radii for the ξ and η directions are given by

$$\lambda_\xi = |uy_\eta - vx_\eta| + c\sqrt{y_\eta^2 + x_\eta^2}, \tag{16}$$

$$\lambda_\eta = |vx_\xi - uy_\xi| + c\sqrt{x_\xi^2 + y_\xi^2}, \tag{17}$$

and c is the speed of sound. The coefficients $\varepsilon^{(2)}$ and $\varepsilon^{(4)}$ use the pressure as a sensor for shocks and stagnation points, and they are defined as

$$\varepsilon_{i+\frac{1}{2},j}^{(2)} = K^{(2)} \max(\nu_{i-1,j}, \nu_{i,j}, \nu_{i+1,j}, \nu_{i+2,j}), \tag{18}$$

$$\nu_{i,j} = \left| \frac{p_{i-1,j} - 2p_{i,j} + p_{i+1,j}}{p_{i-1,j} + 2p_{i,j} + p_{i+1,j}} \right|, \tag{19}$$

$$\varepsilon_{i+\frac{1}{2},j}^{(4)} = \max[0, (K^{(4)} - \varepsilon_{i+\frac{1}{2},j}^{(2)})], \tag{20}$$

where typical values for the constants $K^{(2)}$ and $K^{(4)}$ are $\frac{1}{4}$ and $\frac{1}{128}$, respectively.

For the normal direction (η), the dissipation contributions are defined in a similar way, except

$$(\overline{\lambda}_\eta)_{i,j} = \phi_{i,j}(r^{-1}) \cdot (\lambda_\eta)_{i,j} \tag{21}$$

Care must be taken, especially for internal flows, in defining the smoothing fluxes on the boundary. If the computation of the dissipative terms is carried out in each coordinate direction as the difference between first and third difference operators, conditions on those terms can be imposed at the boundary such that no errors in the conservation property are introduced, globally, by the numerical dissipation [9]. Moreover, such a scheme reduces the presence of undamped modes and guarantees a dissipative behavior for the dissipative operator D.

TIME-STEPPING SCHEME

The system of differential equations of (10) are advanced in time towards the steady-state solution with a four stage Runge-Kutta scheme. This scheme is fourth order accurate in time for the linear problem and second order accurate for the nonlinear problem. It can be written for the time level n in the form

$$\begin{aligned} U^{(0)} &= U^n \\ U^{(1)} &= U^{(0)} + \alpha_1 \Delta t R(U^{(0)}) \\ U^{(2)} &= U^{(0)} + \alpha_2 \Delta t R(U^{(1)}) \\ U^{(3)} &= U^{(0)} + \alpha_3 \Delta t R(U^{(2)}) \\ U^{(4)} &= U^{(0)} + \alpha_4 \Delta t R(U^{(3)}) \\ U^{n+1} &= U^{(4)} \end{aligned} \tag{22}$$

where at the $(q+1)st$ stage we have in the case of a single evaluation of the dissipation

$$R(U^{(q+1)}) = \frac{1}{V}(Q(U^{(q)}) - D(U^{(0)})), \tag{23}$$

and a good set for the coefficients $\alpha_m (m = 1, 4)$ is

$$\alpha_1 = \frac{1}{4},\ \alpha_2 = \frac{1}{3},\ \alpha_3 = \frac{1}{2},\ \alpha_4 = 1. \tag{24}$$

For economy the viscous terms are computed at the first stage and then frozen for the remaining stages. In multigrid computations, the driving scheme must be designed to rapidly damp out high frequency modes. Good high frequency damping properties are obtained with this scheme by evaluating the artificial dissipation terms on the first and second stages and freezing them for the remaining stages [10].

It is also important to note that the Runge-Kutta scheme has the desirable property that the steady-state solution is independent of the time step; therefore, the scheme is particularly amenable to convergence acceleration techniques.

ACCELERATION TECHNIQUES

Three methods are employed to accelerate convergence of the basic explicit time-stepping scheme. These techniques are as follows: 1) local time stepping; 2) residual smoothing; 3) multigrid. They are discussed in the subsequent subsections.

Local Time Stepping

When the interest is only in the steady-state solution, a faster expulsion of disturbances can be achieved by locally varying the time step. In the present work the actual time step limit Δt is computed using

$$\Delta t = c_0 \left(\frac{\Delta t_c \cdot \Delta t_d}{\Delta t_c + \Delta t_d} \right), \tag{25}$$

where Δt_c is the limit due to the convective terms, Δt_d is the limit due to the diffusive terms, and c_0 is a constant usually taken to be the Courant-Friedrichs-Lewy (CFL) number. In particular,

$$\Delta t_c = \frac{V}{\lambda_\xi + \lambda_\eta}, \tag{26}$$

$$\Delta t_d = \frac{V^2}{K_t \mu [(x_\xi^2 + y_\xi^2) + (x_\eta^2 + y_\eta^2)]}, \tag{27}$$

where $\lambda_\xi, \lambda_\eta$ are defined in (16) and (17), respectively, and k_t is a constant that has been set equal to 2.5 based on numerical experiments.

Residual Smoothing

The stability range of the basic time-stepping scheme can be extended using implicit smoothing of the residuals. This technique was first introduced by Lerat [11] for the Lax-Wendroff scheme, and later devised by Jameson [12] for the Runge-Kutta scheme. For two-dimensional flows the residual smoothing can be applied in the form

$$(1 - \epsilon_\xi \nabla_\xi \Delta_\xi)(1 - \epsilon_\eta \nabla_\eta \Delta_\eta) \overline{R}_m = R_m \tag{28}$$

where the residual R_m is defined by

$$\begin{aligned} R_1 &= \alpha_1 \tfrac{\Delta t}{V} [Q(U^{(0)}) - D(U^{(0)})], \\ R_m &= \alpha_m \tfrac{\Delta t}{V} [Q(U^{(m-1)}) - D(U^{(1)})], \\ & \qquad m = 2, 4 \end{aligned} \tag{29}$$

and computed in the Runge-Kutta stage m, and $\overline{R}_m$ is the final residual at stage m after the sequence of smoothing in the ξ and η directions with the coefficients ϵ_ξ and ϵ_η.

The use of constant coefficients in the implicit treatment has proven to be satisfactory (extending the CFL number by a factor of two to three) even for highly stretched meshes, provided additional dissipative support such as enthalpy damping [5] is introduced. However, the use of enthalpy damping, which assumes constant total enthalpy throughout the flow field, precludes the solution of problems with heat transfer effects. The need for enthalpy damping can be eliminated by using variable coefficients ϵ_ξ and ϵ_η that account

for the variation in cell aspect ratio. For the factorization of (28) effective expressions for the coefficients $\epsilon_\xi, \epsilon_\eta$ can be derived by following the procedure of Martinelli in [6]. These expressions are written as

$$\begin{aligned} \epsilon_\xi &= \max\left\{\frac{1}{4}\left[\left(\frac{CFL}{CFL^*}\cdot\frac{\lambda_\xi}{\lambda_\xi+\lambda_\eta}\cdot\phi(r)\right)^2-1\right],0\right\}, \\ \epsilon_\eta &= \max\left\{\frac{1}{4}\left[\left(\frac{CFL}{CFL^*}\cdot\frac{\lambda_\eta}{\lambda_\xi+\lambda_\eta}\cdot\phi(r^{-1})\right)^2-1\right],0\right\}, \end{aligned} \tag{30}$$

where $\phi(r)$ and $\phi(r^{-1})$ are the same quantities defined for the artificial dissipation, CFL is the local Courant number (usually taken to be 5), and the asterisk refers to the unsmoothed scheme.

Multigrid Strategy

Multigrid methods were first introduced for the solution of elliptic problems [13], and later Ni [14] and Jameson [10] applied them to the Euler equations. Actually, multigrid methods can be implemented to obtain improvement in the convergence rate in solving not only the Euler but also the Navier-Stokes equations [6,15]. The basic idea is to use coarser grids to speed up the propagation of the fine grid corrections. The Full Approximation Storage (FAS) scheme in conjunction with the Runge-Kutta time stepping algorithm developed by Jameson [10] has proven to be an effective multigrid technique.

For the multigrid process coarser meshes are obtained by doubling the mesh spacing. On the auxiliary meshes, the solution is initialized as

$$U_{2h}^{(0)} = \frac{\Sigma V_h U_h}{V_{2h}} \tag{31}$$

where the subscript refers to the mesh spacing value and the sum is over the four fine grid cells that compose the $2h$ grid cell. This rule conserves mass, momentum, and energy. On a coarse grid, a forcing function P is added to the governing discrete equations in order to impose the fine grid approximation. After the initialization of the coarse grid solution, this function is computed as follows:

$$P_{2h} = \sum R_h(U_h) - R_{2h}(U_{2h}^{(0)}). \tag{32}$$

Then, the time-stepping scheme on the $(q+1)^{st}$ stage becomes

$$U_{2h}^{(q+1)} = U_{2h}^{(0)} - \alpha_{q+1}\Delta t[R_{2h}(U_{2h}^{(q)}) + P_{2h}^{(0)}]. \tag{33}$$

We can also define a new value R^* for the residual as

$$R_{2h}^* = R_{2h}(U_{2h}) + P_{2h}, \tag{34}$$

collect this value, restrict the solution U_{2h} to the next coarser grid, and repeat the process. The corrections computed on a coarse grid are transferred back to a finer grid with bilinear interpolation.

Two types of simple fixed cycle multigrid strategies are primarily used. They are the V cycle and the W cycle. In the present work, results were obtained with both cycles. The structure of these cycles in the case of four grids is shown in Fig. (2). The W cycle is defined recursively since it becomes complex as the number of grids increases. At a given grid level subiterations (additional time steps) can be performed in both cycles. Moreover, the application of two Runge-Kutta (R-K) steps on the 2h grid and three R-K steps on all succeeding coarser grids is an effective strategy.

In viscous flow calculations the viscous terms are computed also on the coarser grids, while the turbulent viscosity is evaluated only on the finest grid and then determined on each succeeding coarser grid by a simple averaging of surrounding finer grid values. The artificial dissipation model for the finest grid is replaced on the coarser grids with a simple constant coefficient second difference dissipation model. On each grid, the boundary conditions are computed in the same manner and updated at every Runge-Kutta stage. In order to provide an improved initial solution on the finest grid of the sequence of grids in the basic multigrid procedure, the Full Multigrid (FMG) method is employed. With the FMG method the solution is initialized on a coarser grid of the basic sequence of grids and iterated a prescribed number of cycles using the FAS scheme. The solution is then interpolated to the next finer grid. The process is repeated until the finest grid is reached. In the present work, three refinement levels are used. The first and second levels include two and three grids, respectively, and 50 cycles are performed on each. There are five grids in the final level.

RESULTS AND DISCUSSION

Bicircular Arc Cascade

In [14] Ni presented results for inviscid flow over a 20 percent bicircular arc cascade with gap/chord ratio of 2. Then, Chima and Johnson [15] studied a 10 percent bicircular arc cascade for the case of laminar flow. The present numerical method has been used to study the first cascade geometry for laminar and turbulent flow conditions with separation. In Fig. 3(c) the 129×97 H-type grid used for the laminar calculation is presented. The spacing between the wall and the first cell center is 3×10^{-4} chords and 10^{-2} chords is the minimum spacing in the streamwise direction. For this case, the exit Reynolds number $Re_2 = 500$, the exit isentropic Mach number $(M_i)_2 = .5$, and the angle of attack is zero degrees. The second difference artificial dissipation is set to zero. Figure 3(a) shows the

convergence history for the root mean square of the residual of the continuity equation scaled by the initial value. To indicate the monotone behavior of the multigrid scheme, 300 iterations were performed on the finest grid. Using 5 grid levels and a V cycle with subiterations there are 7.2 decades decrease in the residual. In Fig. 3(b), the predicted isentropic Mach number distribution for the viscous solution is compared with that for the inviscid solution. The Euler solution was computed on a grid with the same number of cells but with a minimum spacing in each coordinate direction of 10^{-2} chords. Mach number contours for this case are given in Fig. 3(d). The flow is separated at about the 90 percent chord location. Due to the low Reynolds number, we found that this is one of the cases where it is important to compute the viscous terms on the coarser grids.

Results for transonic turbulent flow ($M_i = 0.675$) are presented in Fig. 4. Figure 4(c) displays the 129×97 mesh used in this test case. The minimum spacing at the wall boundary is 10^{-4} chords, and in the x direction a spacing of about 1.5×10^{-2} chords is used to obtain a good representation of the shock wave. For the inviscid mesh the minimum spacing at the wall is equal to the one in the x direction. Figure 4(a) shows the convergence history for a V cycle with subiterations. The variations in the computed isentropic Mach number are given in Fig. 4(b). In this case, the flow exhibits a little separation, involving about three cells, at the foot of the shock. Then, the flow reattaches and remains so until the 78 percent chord position. The Mach number contours for this flow (Fig. 4(d)) reveal a clean capturing of the shock.

Gas Turbine Rotor Blade

The present numerical method has been tested on several internal flow cases. In order to validate the method for turbomachinery applications, computations were performed for a Von Karman Institute (VKI) gas turbine rotor blade. This blade was tested extensively, as seen in [16,17]. At the inlet the flow angle with the respect to the turbine axes is 30 degrees. The flow is turned about 96 degrees by the blade. For the solutions included herein the inlet Mach number is about 0.27 and the outlet isentropic Mach number $(M_i)_2$ varies from 0.81 to 1.20. Viscous results are compared with inviscid ones and with the available experimental data.

The mesh used for the inviscid calculations is shown in Fig. 5. It is a 145×33 grid with minimum spacing in the x and y directions equal to 1.5×10^{-2} chords. For the viscous computations (Fig. 6) the number of points in the y direction is increased to 65, and the spacing between the blade and the first cell center in the direction normal to the blade is set to 10^{-4} chords. In both the meshes 32 points are located in the x direction before the blade, 65 points on the blade, and 48 points after the blade. A fine mesh is maintained after the blade in order to obtain good resolution of the shock system in the case with

supersonic outlet flow.

In Fig. 7 the convergence history, Mach number distribution, and Mach number contours for the condition $(M_i)_2 = .81$ are displayed. The Navier-Stokes solution is in good agreement with the experimental data. This solution shows less tendency than the Euler one for overexpansion on the pressure side at the trailing edge. Some loss of accuracy in the trailing edge flow can be attributed to the mesh distortion of the H-type grid. Such distortion would also occur for a C-type grid.

Results for transonic conditions $((M_i)_2 = 1.0)$ are presented in Fig. 8. Again, there is good agreement between the viscous result and the experiment. Convergence histories for this case using the W cycle, V cycle with and without subiterations, and the basic scheme (CFL = 2.5) with only local time stepping are given in Fig. 9. Similar convergence behavior is obtained with both the W cycle and the V cycle with subiterations. Approximately the same amount of work (i.e., computer CPU time) is required for each cycle. The performance of the standard V cycle is not as good as that of the V cycle with subiterations. The convergence rate with each multigrid cycle is significantly faster than that of the basic scheme.

In the case of supersonic outlet flow $((M_i)_2 = 1.2)$ the numerical predictions are shown in Fig. 10. The agreement with the experimental measurements is good, and Mach number contours reveal a good resolution of the shock system.

All the cases presented here suggest that engineering accuracy can be achieved in less than 100 multigrid cycles with the finest mesh.

Supersonic Internal Flow

Figures 11 and 12 show results for supersonic flow conditions. The geometry (see Fig. 12) is the same as that investigated by Ni [14]; it is a duct with a 4 percent bump. No experimental data are available for this case, but comparisons between Euler solutions obtained from [14] and those from the present work indicate close agreement. Figures 12(a) and (b) display respectively the viscous and inviscid Mach number contours for an inlet Mach number of 1.4. A 145×97 mesh was used for the viscous calculation, and a 145×33 mesh was used for the inviscid one. For the viscous flow, $\Delta x_{min} = 1.5 \times 10^{-2}$ chords and $\Delta y_{min} = 2 \times 10^{-4}$ chords, and for the inviscid flow, $\Delta x_{min} = \Delta y_{min} = 1.5 \times 10^{-2}$ chords. The two grids have a similar stretching in the y direction; this is why the shocks are smeared in almost the same way. To examine the shock capturing properties of the scheme, an inviscid computation on a weakly stretched 145×65 mesh was performed. As indicated in Fig. 12(c), the shock system is sharply captured with no tendency for smearing. Note that the same input coefficients were used in the dissipation model. Thus, care must be exercised in stretching the mesh when computing flows with strong oblique shocks. Next,

in Fig. 11(b) the Euler and Navier-Stokes solutions for the M_i distribution are presented. This disagreement is probably due to the interactions between shocks and boundary-layers. In fact, all the shocks cause separation at the locations where they impinge on the walls. The convergence history for the viscous case is given in Fig. 11(a).

CONCLUSION

The use of a Runge-Kutta scheme with acceleration techniques has proven to be fast, reliable, and accurate for the study of transonic internal flow. No problems lie in the extension of the numerical method to three-dimensional applications due to the versatility of the H-type grid. In addition, the very good convergence of the full multigrid process indicates the value of the method in turbomachinery component design.

ACKNOWLEDGMENT

The first author would like to express his gratitude to ICASE and NASA for providing facilities and computer time for this work.

References

[1] Chima, R. V., "Inviscid and Viscous Flows in Cascades with an Explicit Multiple-grid Algorithm," AIAA J., Vol. 23, No. 10, October 1985, pp. 1556-1563.

[2] Weinberg, B. C., Yang, R.-J., McDonald, H., and Shamroth, S. J., "Calculations of Two- and Three-dimensional Transonic Cascade Flow Fields Using the Navier-Stokes Equations," ASME Journal of Engineering for Gas Turbines and Power, Vol. 108, January 1986, pp. 93-102.

[3] Schäfer, O., Frühauf, H.-H., Bauer, B., and Guggolz, M. "Application of a Navier-Stokes Analysis to Flows through Plane Cascades," ASME Journal of Engineering for Gas Turbines and Power, Vol. 108, January 1986, pp. 103-111.

[4] Baldwin, B. S. and Lomax, H., "Thin Layer Approximation and Algebraic Model for Separated Turbulent Flows," AIAA Paper No. 78-257, January 1978.

[5] Swanson, R. C. and Turkel, E., "A Multistage Time-stepping Scheme for the Navier-Stokes Equations," AIAA Paper 85-0035, January 1985.

[6] Martinelli, L., "Calculations of Viscous Flows with a Multigrid Method," Ph.D. Dissertation, MAE Department, Princeton University, October 1987.

[7] Jameson, A., Schmidt, W., and Turkel, E., "Numerical Solutions of the Euler Equations by Finite Volume Methods Using Runge-Kutta Time-stepping Schemes," AIAA Paper 81-1259, June 1981.

[8] Swanson, R. C. and Turkel, E., "Artificial Dissipation and Central Difference Schemes for the Euler and Navier-Stokes Equations," AIAA Paper 87-1107, AIAA 8th Computational Fluid Dynamics Conference, Honolulu, Hawaii, June 9-11, 1987.

[9] Holmes, D. G. and Tong, S. S., "A Three-dimesional Euler Solver for Turbomachinery Blade Rows," Transactions of the ASME, Vol. 107, April 1985.

[10] Jameson, A., "Transonic Flow Calculations," MAE Report 1651, MAE Department, Princeton University, July 1983.

[11] Lerat, A., "Une Classe de Schémas aux Différences Implicites Pour les Systèmes Hyperboliques de lois de Conservation," *Comptes Rendus Acad. Sciences Paris*, Vol. 288A, 1979.

[12] Jameson, A., "The Evolution of Computational Methods in Aerodynamics," J. Appl. Mech., Vol. 50, 1983.

[13] Brandt, A., "Multi-Level Adaptive Computations in Fluid Dynamics," AIAA Paper 79-1455, 1979.

[14] Ni, R.-H., "Multiple-Grid Scheme for Solving the Euler Equations," AIAA Paper 81-1025, June 1981.

[15] Chima, R. V. and Johnson, G. M., "Efficient Solution of the Euler and Navier-Stokes Equations with a Vectorized Multiple-Grid Algorithm," AIAA J., Vol. 23, No. 1, January 1985, pp. 23-32.

[16] Sieverding, C. H., "Experimental Data on Two Transonic Turbine Blade Sections and Comparisons with Various Theoretical Methods," Von Kárman Institute for Fluid Dynamics, Report LS59, 1973.

[17] Kiock, R., Lehthaus, F., Baines, N. C., and Sieverding, C. H., "The Transonic Flow through a Plane Turbine Cascade as Measured in Four European Wind Tunnels," ASME Journal of Engineering for Gas Turbines and Power, Vol. 108, April 1986, pp. 277-284.

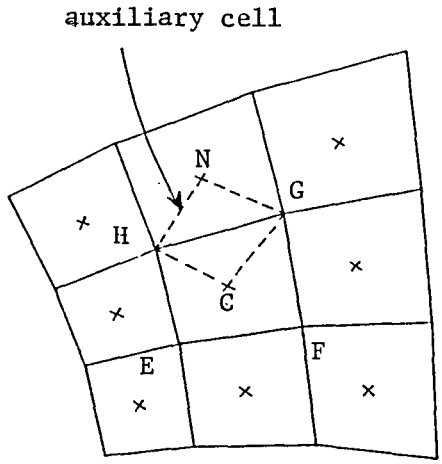

Fig. 1: Auxiliary cell for computation of viscous terms.

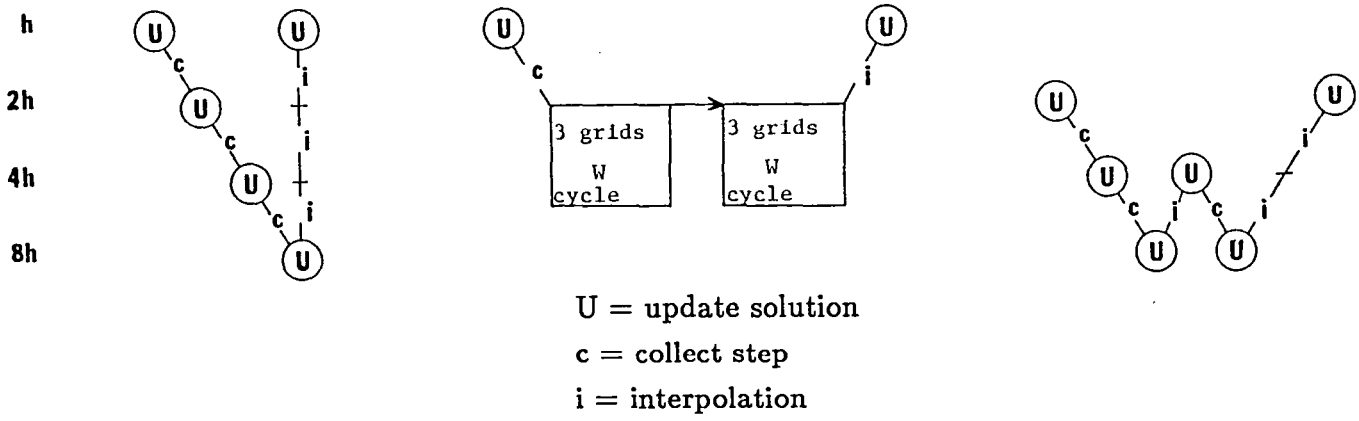

Fig. 2: Schematic of V and W cycles with 4 grids.

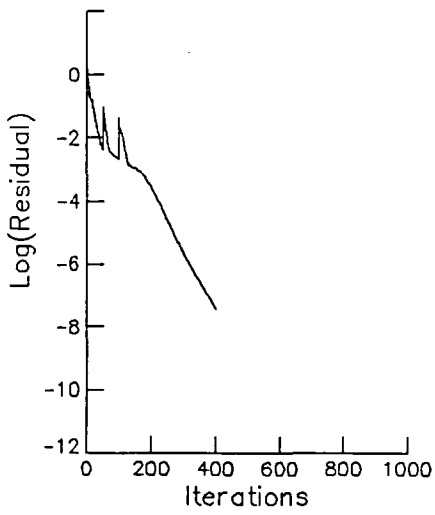

a) Convergence history
V cycle with
subiterations

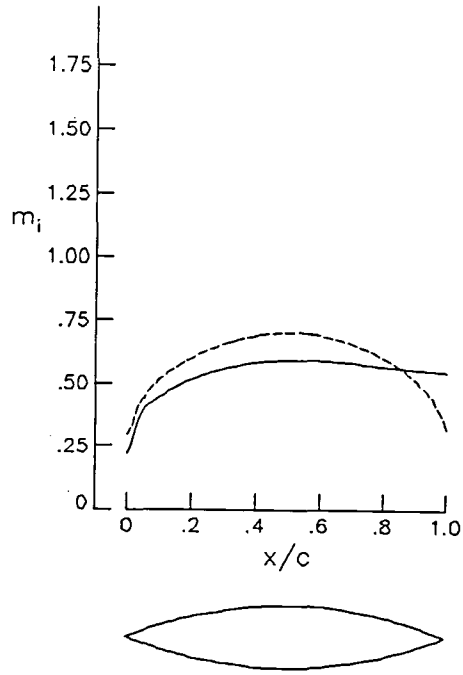

b) Isentropic Mach number
distribution
- - - Euler
—— Navier-Stokes

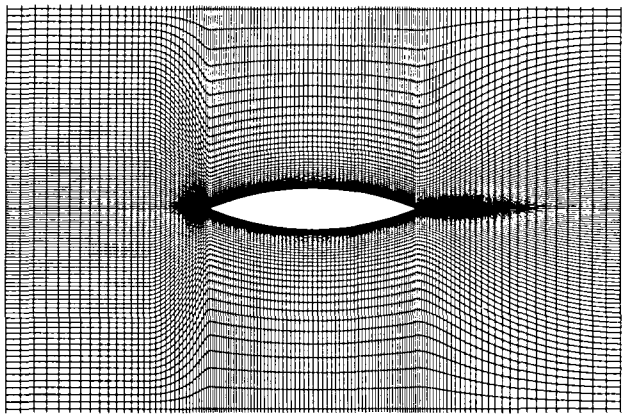

c) 129 × 97 laminar flow grid

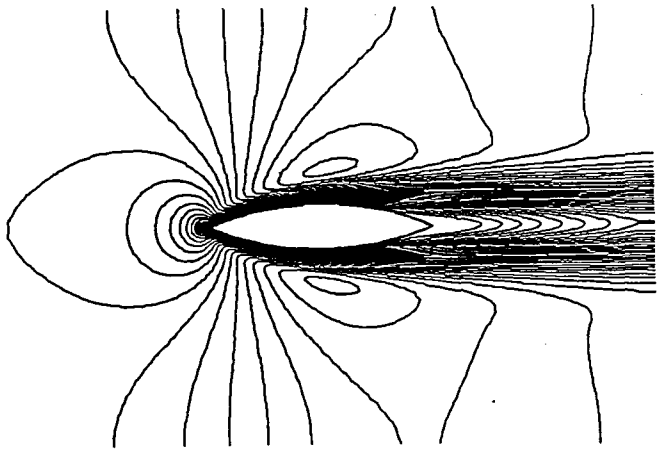

d) Mach number contours

Fig. 3: Bicircular arc cascade ($(M_i)_2 = .5; Re_2 = 500$).

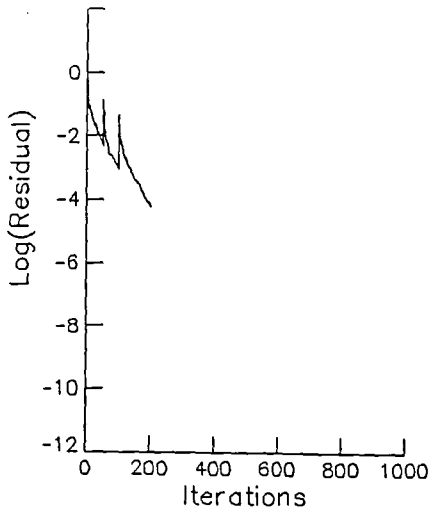

a) Convergence history
V cycle with
subiterations

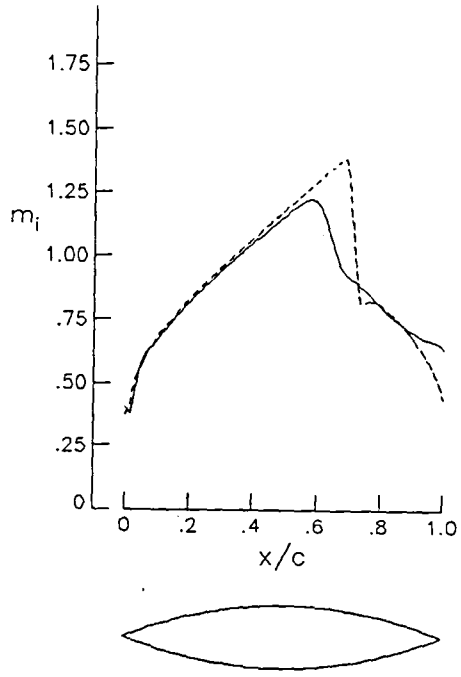

b) Isentropic Mach number
distribution
- - - Euler
—— Navier-Stokes

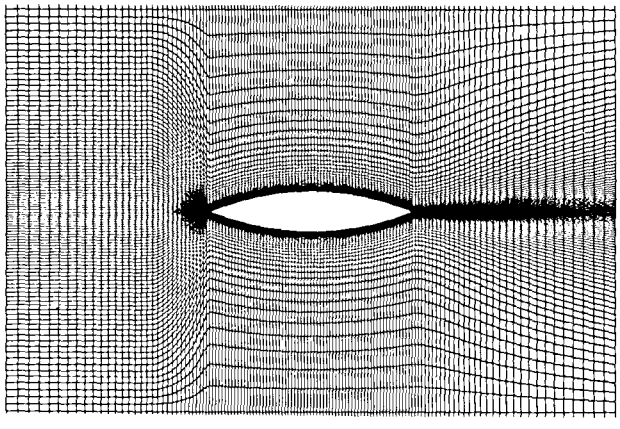

c) 129 × 97 turbulent flow grid

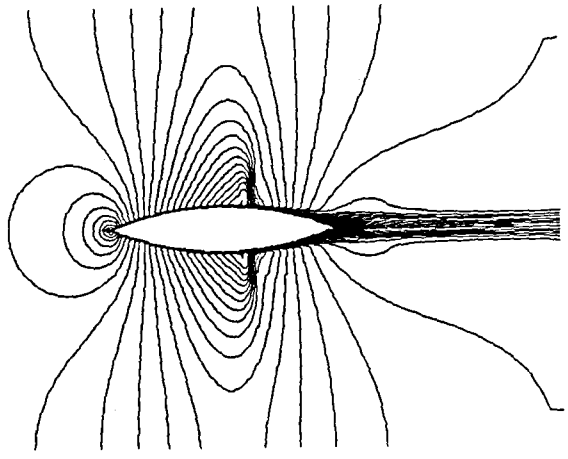

d) Mach number contours

Fig. 4: Bicircular arc cascade ($(M_i)_2 = .675; Re_2 = 1 \times 10^6$).

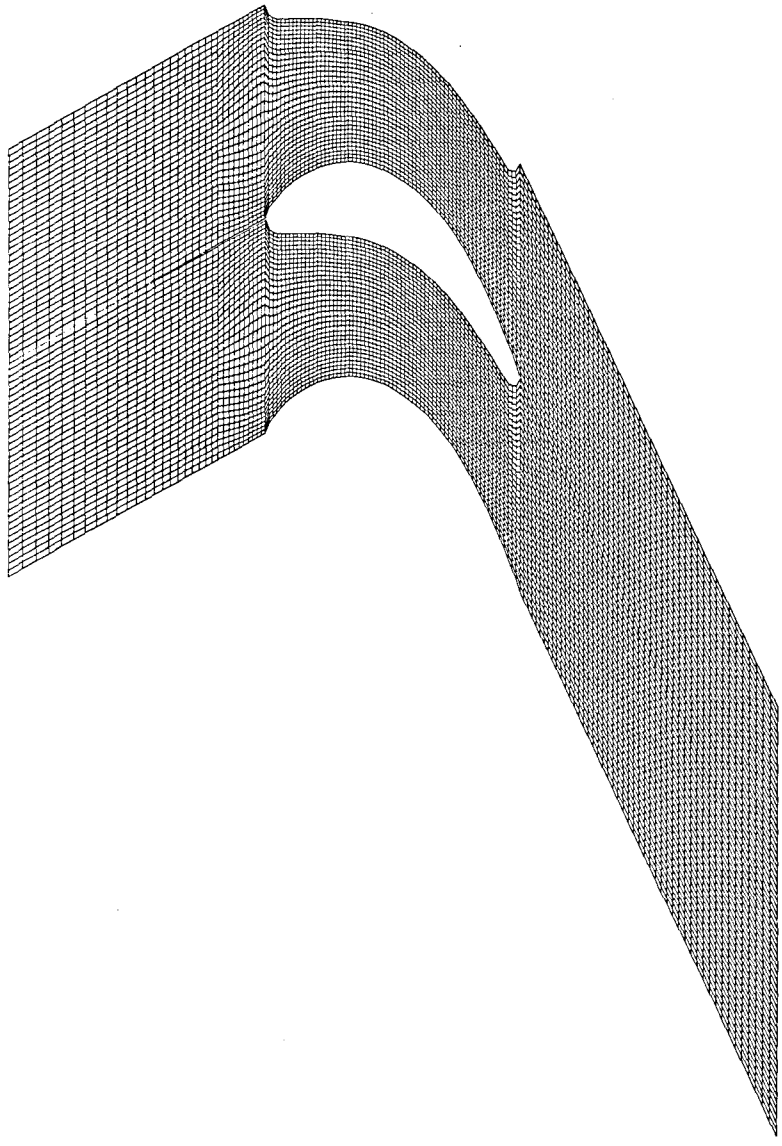

Fig. 5: 145×33 inviscid flow mesh for VKI LS59 gas turbine rotor blade.

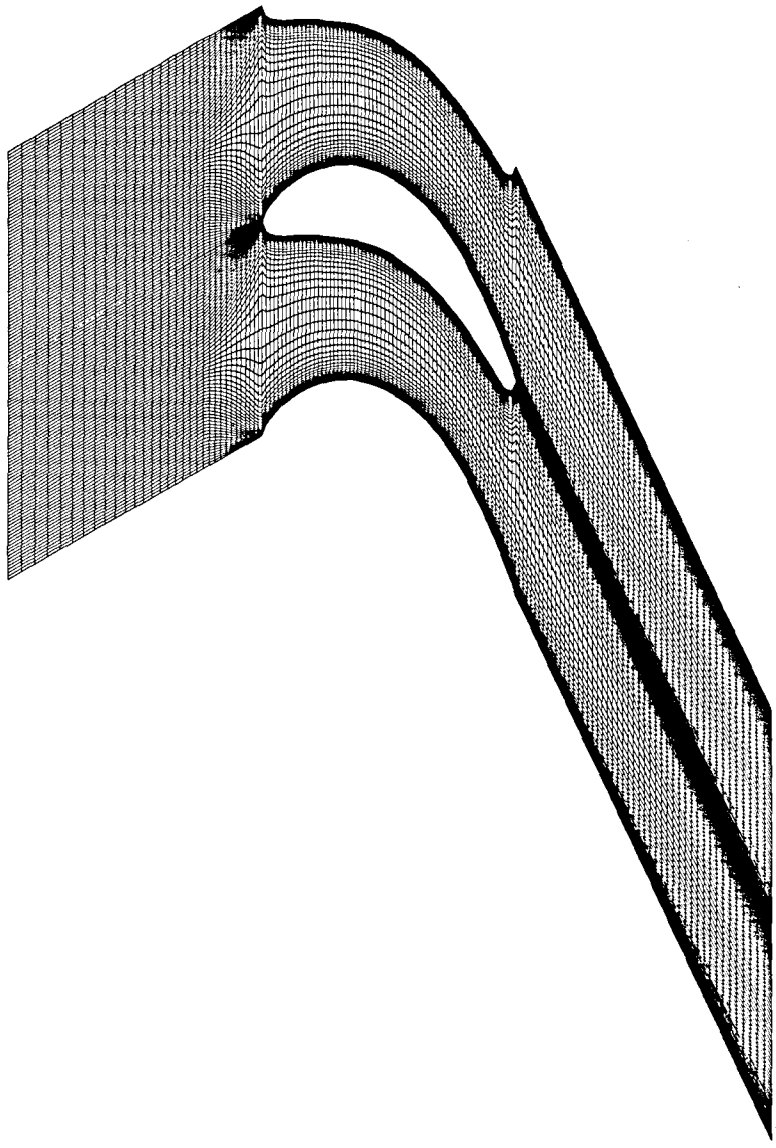

Fig. 6: 145×65 viscous flow mesh for VKI LS59 gas turbine rotor blade.

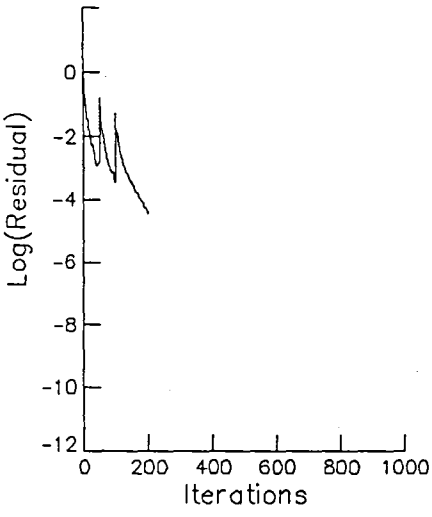

a) Convergence history
W cycle

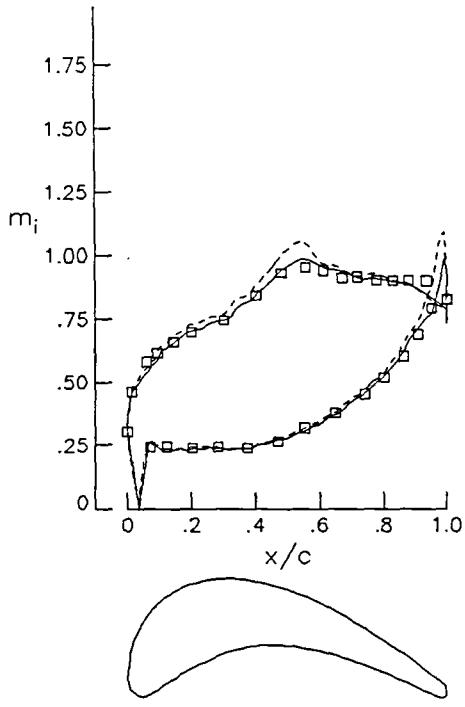

b) Isentropic Mach number distribution
- - - Euler
—— Navier-Stokes
□ Experiment Ref. [16,17]
$\alpha_1 = 30°$
$(M_i)_2 = .81$
$Re_2 = 8 \times 10^5$

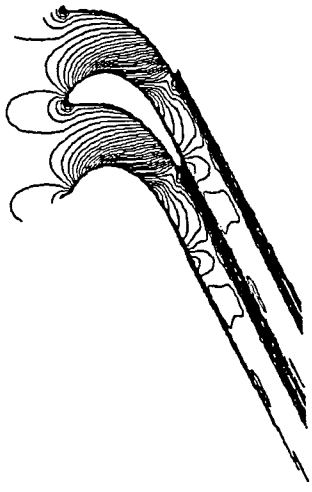

c) Mach number contours

Fig. 7: VKI LS59 turbine blade ($(M_i)_2 = .81$).

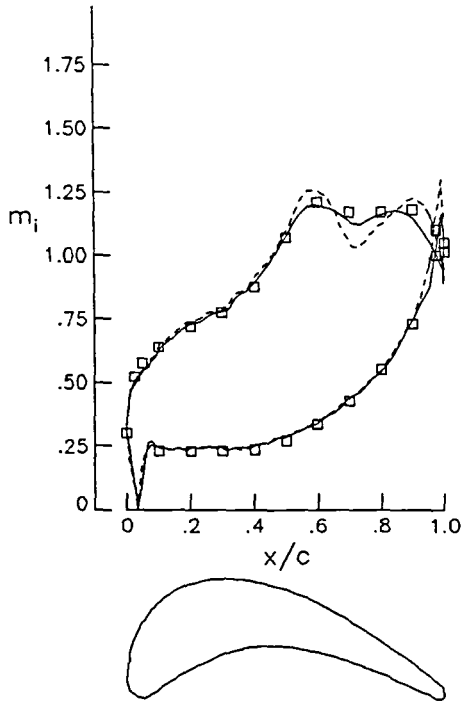

a) Isentropic Mach number distribution

- - - Euler

—— Navier-Stokes

□ Experiment Ref. [16,17]

$\alpha_1 = 30°$

$(M_i)_2 = 1.$

$Re_2 = 8 \times 10^5$

b) Mach number contours

Fig. 8: VKI LS59 turbine blade ($(M_i)_2 = 1$).

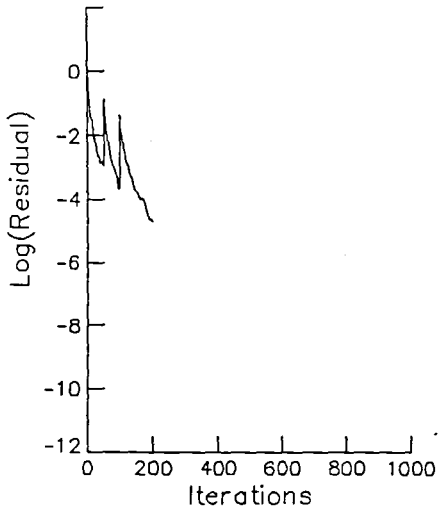

a) W cycle

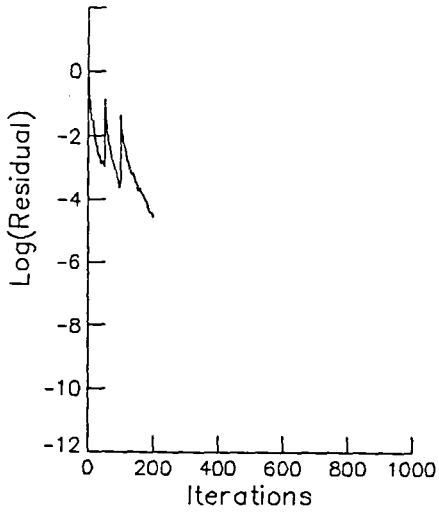

b) V cycle with subiterations

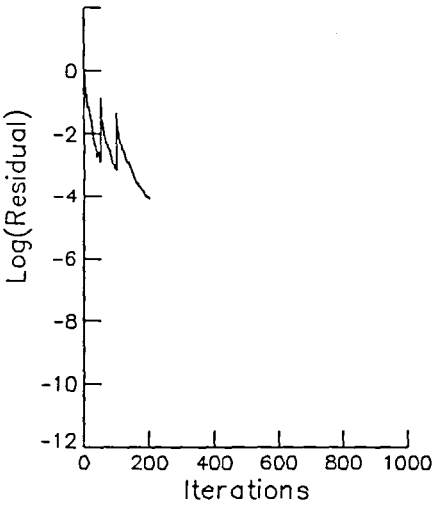

c) Standard V cycle

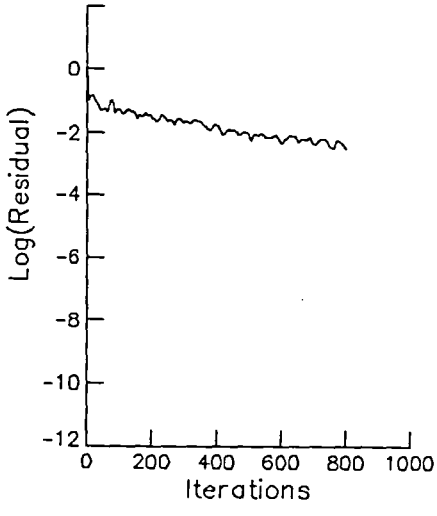

d) Basic scheme CFL = 2.5

Fig. 9: Convergence histories for VKI LS59 turbine blade ($(M_i)_2 = 1$).

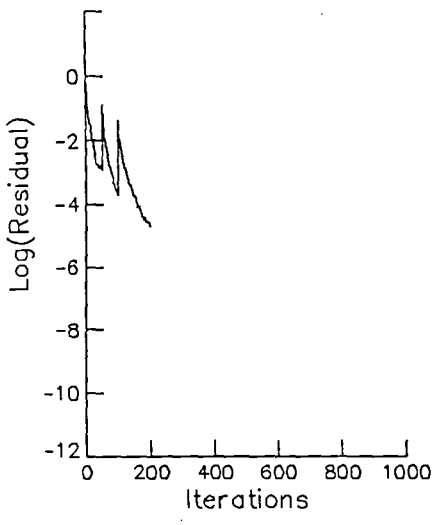

a) Convergence history
W cycle

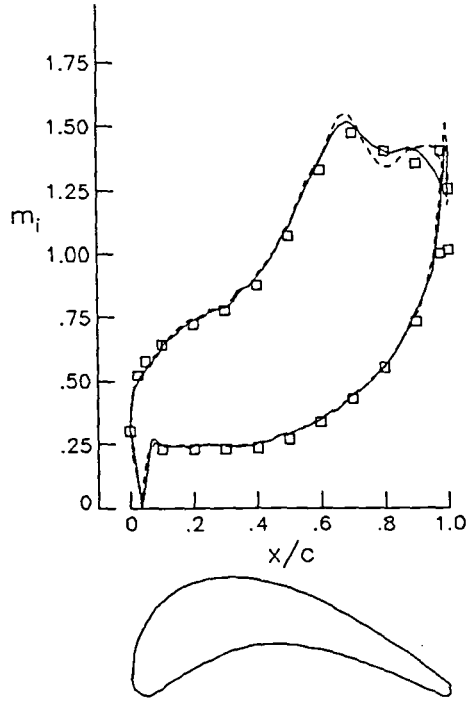

b) Isentropic Mach number distribution
- - - Euler
—— Navier-Stokes
□ Experiment Ref. [16,17]
$\alpha_1 = 30°$
$(M_i)_2 = 1.2$
$Re_2 = 8 \times 10^5$

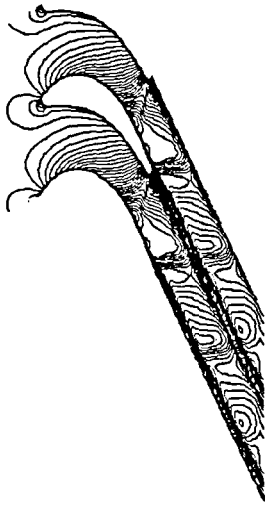

c) Mach number contours

Fig. 10: VKI LS59 turbine blade ($(M_i)_2 = 1.2$).

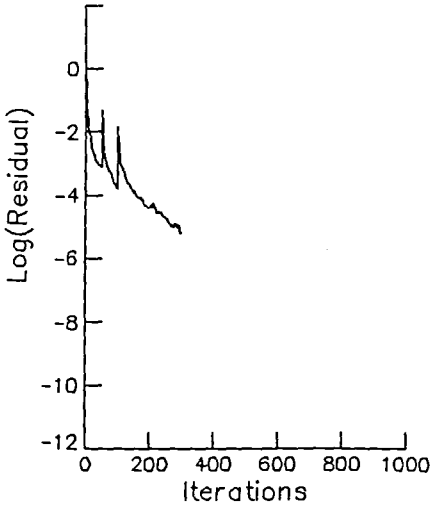

a) Convergence history
V cycle with
subiterations

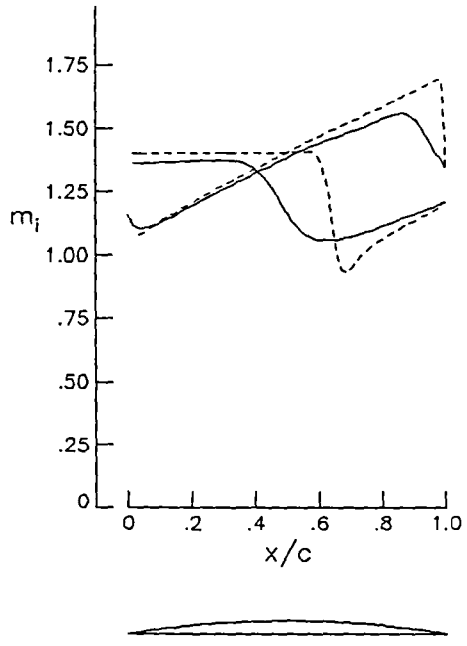

b) Isentropic Mach number
distribution
- - - Euler
—— Navier-Stokes

Fig. 11: Supersonic internal flow ($M_1 = 1.4$).

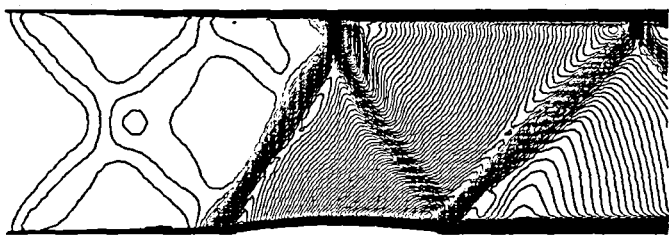

a) Viscous Mach number contours

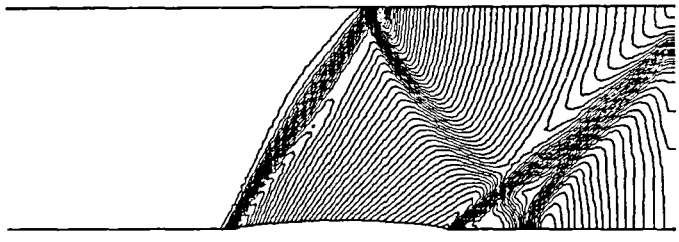

b) Inviscid Mach number contours

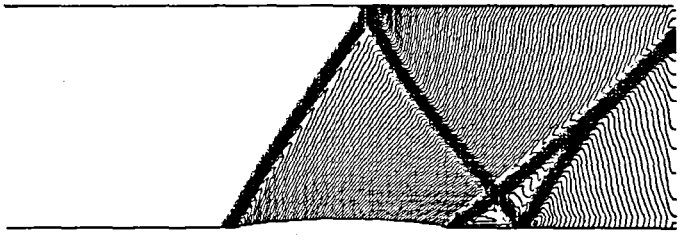

c) Inviscid Mach number contours on weakly stretched mesh

Fig. 12: Supersonic internal flow ($M_1 = 1.4$).

NASA
National Aeronautics and Space Administration

Report Documentation Page

1. Report No.	2. Government Accession No.	3. Recipient's Catalog No.
NASA CR-181682 ICASE Report No. 88-32		

4. Title and Subtitle	5. Report Date
A NAVIER-STOKES SOLVER FOR CASCADE FLOWS	July 1988
	6. Performing Organization Code

7. Author(s)	8. Performing Organization Report No.
A. Arnone and R. C. Swanson	88-32
	10. Work Unit No. 505-90-21-01

9. Performing Organization Name and Address	11. Contract or Grant No.
Institute for Computer Applications in Science and Engineering Mail Stop 132C, NASA Langley Research Center Hampton, VA 23665-5225	NAS1-18107
	13. Type of Report and Period Covered: Contractor Report

12. Sponsoring Agency Name and Address	14. Sponsoring Agency Code
National Aeronautics and Space Administration Langley Research Center Hampton, VA 23665-5225	

15. Supplementary Notes

Langley Technical Monitor:
Richard W. Barnwell

Final Report

Submitted to Journal of Engineering for Gas Turbines and Power

16. Abstract

A computer code for solving the Reynolds averaged full Navier-Stokes equations has been developed and applied using sheared H-type grids. The Baldwin-Lomax eddy-viscosity model is used for turbulence closure. The integration in time is based on an explicit four-stage Runge-Kutta scheme. Local time stepping, variable coefficient implicit residual smoothing, and a full multigrid method have been implemented to accelerate steady state calculations. Comparisons with experimental data show that the code is an accurate viscous solver and can give very good blade-to-blade predictions for engineering applications in less than 100 multigrid cycles on the finest mesh.

17. Key Words (Suggested by Author(s))	18. Distribution Statement
Navier-Stokes, cascade	34 - Fluid Mechanics and Heat Transfer 64 - Numerical Analysis Unclassified - unlimited

19. Security Classif. (of this report)	20. Security Classif. (of this page)	21. No. of pages	22. Price
Unclassified	Unclassified	27	A03

End of Document